η photoproduction on the proton in a chiral constituent quark approach via a one-gluon-exchange model

Jun He,[1,2] B. Saghai,[1,*] and Zhenping Li[3]

[1]*Institut de Recherche sur les lois Fondamentales de l'Univers, DSM/IRFU, CEA/Saclay, F-91191 Gif-sur-Yvette, France*

[2]*Institut of Modern Physics, Chinese Academy of Sciences, Lanzhou 730000, People's Republic of China*

[3]*Department of Computer and Information Science, University of Maryland, Maryland 20783, USA*

(Received 26 February 2008; published 17 September 2008)

A formalism based on a chiral quark model (χQM) approach complemented with a one-gluon-exchange model, to take into account the breakdown of the SU(6)⊗O(3) symmetry, is presented. The configuration mixing of wave functions for nucleon and resonances are derived. With few adjustable parameters, differential cross-section and polarized-beam asymmetry for the $\gamma p \to \eta p$ process are calculated and successfully compared with the data in the center-of-mass energy range from threshold to 2 GeV. The known resonances $S_{11}(1535)$, $S_{11}(1650)$, $P_{13}(1720)$, $D_{13}(1520)$, and $F_{15}(1680)$, as well as two new S_{11} and D_{15} resonances, are found to be dominant in the reaction mechanism. Moreover, connections among the scattering amplitudes of the χQM approach and the helicity amplitudes, as well as decay widths of resonances, are established. Possible contributions from the so-called missing resonances are investigated and found to be negligible.

DOI: 10.1103/PhysRevC.78.035204 PACS number(s): 14.20.Gk, 13.60.Le, 12.39.Fe, 12.39.Jh

I. INTRODUCTION

Electromagnetic production of mesons on the nucleon offers a great opportunity to deepen our understanding of the baryon resonances properties. In recent years, intensive experimental efforts have been devoted to the measurement of observables for the processes of pseudoscalar and vector-meson production, using electron and/or photon beam facilities.

In the present work we investigate the reaction $\gamma p \to \eta p$, in the range of center-of-mass total energy from threshold up to $W \approx 2$ GeV, to interpret a large amount of high-quality data released from various facilities, namely differential cross-section data by the following collaborations: MAMI [1], CLAS [2], CB-ELSA [3], LNS-GeV-γ [4], and GRAAL [5], and polarized beam asymmetries by CB-ELSA/TAPS [6] and GRAAL [5].

The copious set of data has motivated extensive theoretical investigations. Most of the available models are based on meson-nucleon degrees of freedom, in which the Feynman diagrammatic techniques are used so the transition amplitudes are Lorentz invariant. In recent years various advanced approaches have been developed, namely the unitary isobar model of MAID [7], Giessen [8], and Bonn-Gatchina groups [9] coupled-channel approaches, as well as the partial-wave analysis of SAID [10]. Those approaches have no explicit connection with quantum chromodynamics (QCD), and the number of free parameters in the models increases with the number of included resonances.

Formalisms embodying the subnucleonic degrees of freedom are also being developed (for a recent review see Ref. [11]). Such a program has its genesis in early 1970s due to the works by Copley, Karl, and Obryk [12] and Feynman, Kisslinger, and Ravndal [13] in the pion photoproduction, who provided the first clear evidence of the underlying SU(6)⊗O(3) structure of the baryon spectrum. Soon after, in a seminal article, Du Rújula, Georgi, and Glashow [14] attributed the appearance of SU(6)⊗O(3) supermultiplets to the color gauge couplings generating a long-range spin-independent force. Based on those investigations, since late 1970s excited baryon states have been intensively studied. The most extended and phenomenologically successful approach was developed by Isgur, Karl, and Koniuk [15–19] in the framework of a nonrelativistic quark potential formalism. The dynamical degrees of freedom, appropriate to low-mometum transfer, are constituent (valence) quarks with effective masses of about 330 MeV for u and d quarks. The confining potential is created by the gluon fields. Although the nonrelativistic approach suffers from several flaws (see, e.g., Ref. [11]), its surprising capability in providing a coherent undestanding of the low-energy phenomena of the baryon spectroscopy is very likely due to the choice of *effective* parameters, such as constituent-quark mass, the string tension, and the coupling α_s. Those points were investigated by Capstick and Isgur [20] in their relativized quark model approach for baryons. This latter formalism was used by Capstick and Roberts [21–23] in comprehensive calculations of strong decay amplitudes. More recently, a further step was taken [24] to go beyond the simplest qqq Fock space configuration and include qqq-$q\bar{q}$ components. Such issues turn out to be crucial [25] in comparing mass spectrum generated by quark models with the resonance masses reported in Particle Data Group (PDG) [26].

Those constituent qurak approaches embody one-gluon-exchange (OGE) dynamics. Generalizing one-pion-exchange (OPE) mechanism, an alternative to that scheme has been developed by Glozman and Riska [27] according to which the spin-dependent coupling between costituent quarks arises from Goldstone-boson-exchange (GBE). Then a debate emerged [28,29] on the OGE versus OPE as the most

*bijan.saghai@cea.fr

appropriate effective degree of freedom. Although at the present time no firm conclusions can be drawn [30–33], there are indications in favor of OGE [34–36].

The approaches mentioned above, as well as other QCD-inspired ones, reviewed in Ref. [11], have concentrated mainly on the transition amplitudes and the baryon mass spectrum. In the present work we study those issues and go further, investigating also reaction mechanism of the process $\gamma p \to \eta p$.

In Ref. [37] a comprehensive and unified approach to the pseudoscalar mesons photoproduction, based on the low-energy QCD Lagrangian [38], is developed with the explicit quark degrees of freedom. This approach reduces drastically the number of free parameters, for example, within the exact SU(6)⊗O(3) symmetry, the reaction under investigation has only one free parameter, namely ηNN coupling constant. However, that symmetry is broken and to take into account that effect, one free parameter per resonance was introduced in previous calculations [39,40]. Given that the configuration mixing among the three-constituent quarks bound states is a consequence of the SU(6)⊗O(3) symmetry breakdown, in the present work we use the one-gluon-exchange mechanism to generate the configuration mixing of the wave functions. In this approach, the number of parameters decreases significantly. After the parameters are determined by fitting the data, we then study the contributions from the missing resonances (see, e.g., Refs. [11,41,42]). Moreover, we give relations connecting the scattering amplitudes in our χQM approach to the photoexcitation helicity amplitudes and partial decay widths of resonances. Our approach offers also the opportunity of investigating new nucleon resonances, for which strong indications have been reported in the literature [9,40,42–51].

As mentioned earlier, the choice of effective degrees of freedom is not unique. In this work we adopt the OGE mechanism within the Isgur-Karl nonreletavistic quarks potential formulation, proven to offer a successful phenomenological frame. Nevertheless, our results are to be considered as semiquantitaive, awaiting the extension of our approach to more sophisticated quark models.

The article is organized as follows. In Sec. II, the theoretical content of our work is presented. Starting from a chiral effective Lagrangian, the Chew-Goldberger-Low-Nambu (CGLN) amplitudes for the process $\gamma p \to \eta p$ are given within the SU(6)⊗O(3) symmetry. Then the consequences of the breaking of that symmetry *via* configuration mixing in OGE model is reported and helicity amplitudes of photon transition and meson decay partial widths of resonances are presented. The fitting procedure and numerical results for differential cross-section, polarized beam asymmetry, helicity amplitudes, and $N^* \to \eta N$ partial decay widths are reported and discussed in Sec. III, where possible roles played by new/missing resonances are examined. Summary and conclusions are given in Sec. IV.

II. THEORETICAL FRAME

In this section we recall the content of a chiral constituent quark approach and relate it to the configuration mixing of constituent quarks states *via* a OGE model, generated by the breakdown of the SU(6)⊗O(3) symmetry. Then we present issues related to the photoexcitation helicity amplitudes and the partial decay widths of nucleon resonances.

A. Chiral constituent quark model

As in Ref. [37], we start from an effective chiral Lagrangian [38],

$$\mathcal{L} = \bar{\psi}[\gamma_\mu(i\partial^\mu + V^\mu + \gamma_5 A^\mu) - m]\psi + \cdots, \tag{1}$$

where vector (V^μ) and axial (A^μ) currents read,

$$V^\mu = \frac{1}{2}(\xi\partial^\mu\xi^\dagger + \xi^\dagger\partial^\mu\xi), \quad A^\mu = \frac{1}{2i}(\xi\partial^\mu\xi^\dagger - \xi^\dagger\partial^\mu\xi), \tag{2}$$

where $\xi = \exp(i\Pi/f_m)$ and f_m is the meson decay constant. ψ and ϕ_m are the quark and meson fields, respectively. The field Π is a $3 \otimes 3$ matrix,

$$\Pi = \begin{vmatrix} \frac{1}{\sqrt{2}}\pi^\circ + \frac{1}{\sqrt{6}}\eta & \pi^+ & K^+ \\ \pi^- & -\frac{1}{\sqrt{2}}\pi^\circ + \frac{1}{\sqrt{6}}\eta & K^\circ \\ K^- & \bar{K}^\circ & -\sqrt{\frac{2}{3}}\eta \end{vmatrix}, \tag{3}$$

in which the pseudoscalar mesons, π, K, and η, are treated as Goldstone bosons so the Lagrangian in Eq. (1) is invariant under the chiral transformation. Therefore, there are four components for the photoproduction of pseudoscalar mesons based on the QCD Lagrangian,

$$\mathcal{M}_{fi} = \langle N_f|H_{m,e}|N_i\rangle + \sum_j \left\{ \frac{\langle N_f|H_m|N_j\rangle\langle N_j|H_e|N_i\rangle}{E_i + \omega - E_j} + \frac{\langle N_f|H_e|N_j\rangle\langle N_j|H_m|N_i\rangle}{E_i - \omega_m - E_j} \right\} + \mathcal{M}_T, \tag{4}$$

where $N_i(N_f)$ is the initial (final) state of the nucleon, and $\omega(\omega_m)$ represents the energy of incoming (outgoing) photons (mesons). The pseudovector and electromagnetic couplings at the tree level are given, respectively, by the following standard expressions:

$$H_m = \sum_j \frac{1}{f_m}\bar{\psi}_j\gamma_\mu^j\gamma_5^j\psi_j\partial^\mu\phi_m;$$

$$H_e = -\sum_j e_j\gamma_\mu^j A^\mu(\mathbf{k},\mathbf{r}), \tag{5}$$

where $A^\mu(\mathbf{k},\mathbf{r})$ is the electromagnetic field. The first term in Eq. (4) is a seagull term. It is generated by the gauge transformation of the axial vector A_μ in the QCD Lagrangian. This term, being proportional to the electric charge of the outgoing mesons, does not contribute to the production of the η meson. The second and third terms correspond to the s and u channels, respectively. The last term is the t-channel contribution.

In this article we focus on the nucleon resonance contributions. Given that the u-channel contributions are less sensitive to the details of resonances structure than those in the

s channel, it is then reasonable to treat the u-channel components as degenerate [40].

For the s channel, the amplitudes are given by the following expression [37,40]:

$$\mathcal{M}_{N^*} = \frac{2M_{N^*}}{s - M_{N^*}^2 - iM_{N^*}\Gamma(\mathbf{q})} e^{-\frac{\mathbf{k}^2+\mathbf{q}^2}{6\alpha^2}} \mathcal{O}_{N^*}, \tag{6}$$

where $\sqrt{s} \equiv W = E_N + \omega_\gamma = E_f + \omega_m$ is the total center-of-mass energy of the system, and $\mathcal{O}_{N^*}$ is determined by the structure of each resonance. $\Gamma(\mathbf{q})$ in Eq. (6) is the total width of the resonance, and a function of the final-state momentum $\mathbf{q}$.

The transition amplitude for the n^{th} harmonic-oscillator shell is

$$\mathcal{O}_n = \mathcal{O}_n^2 + \mathcal{O}_n^3. \tag{7}$$

The first (second) term represents the process in which the incoming photon and outgoing meson are absorbed and emitted by the same (different) quark.

In the present work, we use the standard multipole expansion of the CGLN amplitudes [52] and obtain the partial-wave amplitudes of resonance $l_{2I,2I\pm1}$. Then, the transition amplitude takes the following form:

$$\begin{aligned}\mathcal{O}_{N^*} = {} & if_{1l\pm}\sigma\cdot\epsilon + f_{2l\pm}\sigma\cdot\hat{\mathbf{q}}\sigma\cdot(\hat{\mathbf{k}}\times\epsilon) \\ & + if_{3l\pm}\sigma\cdot\hat{\mathbf{k}}\hat{\mathbf{q}}\cdot\epsilon + if_{4l\pm}\sigma\cdot\hat{\mathbf{q}}\epsilon\cdot\hat{\mathbf{q}}.\end{aligned} \tag{8}$$

Expressing the CGLN amplitudes in their usual formulation [53,54], leads to the Hebb-Walker amplitudes in terms of photoexcitation helicity amplitudes,

$$A_{l\pm} = \mp f A_{1/2}^{N^*}, \tag{9}$$

$$B_{l\pm} = \pm f\sqrt{\frac{4}{l(l+2)}} A_{3/2}^{N^*}, \tag{10}$$

where

$$\begin{aligned} f &= \frac{1}{(2J+1)2\pi}\left[\frac{M_N E_N}{M_{N^*}^2}k\right]^{1/2} \frac{2M_{N^*}}{s - M_{N^*}^2 + iM_{N^*}\Gamma(\boldsymbol{q})} A_{1/2}^m \\ &\equiv f_0 \frac{2M_{N^*}}{s - M_{N^*}^2 + iM_{N^*}\Gamma(\boldsymbol{q})}, \end{aligned} \tag{11}$$

with $A_{1/2}^m$ the $N^* \to \eta N$ decay amplitude, appearing in the partial decay width,

$$\Gamma_m = \frac{1}{(2J+1)}\frac{|\mathbf{q}|E_N}{\pi M_{N^*}}\left|A_{1/2}^m / C_{mN}^I\right|^2, \tag{12}$$

where $C_{\pi N}^I$ represents the Clebsch-Gordan coefficients related to the isospin coupling in the outgoing channel.

In Ref. [37], the partial decay amplitudes are used to separate the contribution of the state with the same orbital angular momentum L. In fact, with the helicity amplitudes of photon transition and meson decay we can directly obtain the CGLN amplitudes for each resonances in terms of Legendre polynomials derivatives:

$$\begin{aligned} f_{1l\pm} &= f_0\left[\mp A_{1/2}^{N^*} - \sqrt{\frac{l+1/2\mp1/2}{l+1/2\pm3/2}}A_{3/2}^{N^*}\right]P'_{\ell\pm1}, \\ f_{2l\pm} &= f_0\left[\mp A_{1/2}^{N^*} - \sqrt{\frac{l+1/2\pm3/2}{l+1/2\mp1/2}}A_{3/2}^{N^*}\right]P'_{\ell}, \\ f_{3l\pm} &= \pm f_0\frac{2A_{3/2}^{N^*}}{\sqrt{(l-1/2\pm1/2)(l+3/2\pm1/2)}}P''_{\ell\pm1}, \\ f_{4l\pm} &= \mp f_0\frac{2A_{3/2}^{N^*}}{\sqrt{(l-1/2\pm1/2)(l+3/2\pm1/2)}}P''_{\ell}. \end{aligned} \tag{13}$$

All f_is are proportional to the meson decay amplitudes. So they can be used to separate the contributions from the state with the same N and L as presented in Ref. [37].

In our approach, the photoexcitation helicity amplitudes $A_{1/2}^{N^*}$ and $A_{3/2}^{N^*}$, as well as the decay amplitudes, are related to the matrix elements of the electromagnetic interaction Hamiltonian [12],

$$A_\lambda = \sqrt{\frac{2\pi}{k}}\left\langle N^*; J\lambda|H_e|N; \frac{1}{2}\lambda - 1\right\rangle, \tag{14}$$

$$A_\nu^m = \left\langle N; \frac{1}{2}\nu|H_m|N^*; J\nu\right\rangle. \tag{15}$$

B. Configuration mixing

The amplitudes in Sec. II A are derived under the SU(6)⊗O(3) symmetry. However, for physical states that symmetry is broken. An example is the violation of the Moorhouse rule [55]. In Ref. [39], a set of parameters C_{N^*} were hence introduced to take into account the breaking of that symmetry, via following substitution:

$$\mathcal{O}_{N^*} \to C_{N^*}\mathcal{O}_{N^*}. \tag{16}$$

In Refs. [39,40], those parameters were allowed to vary around their SU(6)⊗O(3) values ($|C_{N^*}| = 0$ or 1). In this work, instead of using those adjustable parameters, we introduce the breakdown of that symmetry through the configuration mixing of baryon wave functions.

To achieve such an improvement, we must choose a potential model. As discussed in the Introduction, the most popular ones are the OGE model [16–18] and the Goldstone boson exchange model [27]. As shown in Refs. [31,32], these two models give similar mixing angles for the negative-parity resonances and the relevant observables. Here, we adopt the OGE model that has been successfully used to study the helicity amplitudes and decay widths [19] of resonances.

In OGE model, the Hamiltonian of system can be written as [16–18],

$$\begin{aligned} H = {} & \sum_{i=1}^{3} m_i + \sum_{i=1}^{3}\frac{p_i^2}{2m_i^2} + \sum_{i<j=1}^{3}\frac{1}{2}Kr_{ij}^2 \\ & + \sum_{i<j=1}^{3} U(r_{ij}) + H_{\rm hyp}, \end{aligned} \tag{17}$$

where the m_i is the "constituent" effective masse of quark i and $r_{ij} = r_i - r_j$ the separation between two quarks. The confinement potential has two components: one written as a harmonic oscillator potential ($\frac{1}{2}Kr_{ij}^2$, with K the spring constant) and an unspecified anharmonicity $U(r_{ij})$, treated as a perturbation.

The hyperfine part interaction is the sum of contact and tensor terms,

$$H_{\rm hyp} = \frac{2\alpha_s}{3m_q^2}\sum_{i<j=1}^{3}\left\{\frac{8\pi}{3}\,\mathbf{S}_i\cdot\mathbf{S}_j\,\delta^3(\mathbf{r}_{ij}) + \frac{1}{r_{ij}^3}\left[\frac{3\mathbf{S}_i\cdot\mathbf{r}_{ij}\mathbf{S}_j\cdot\mathbf{r}_{ij}}{\mathbf{r}_{ij}^2} - \mathbf{S}_i\cdot\mathbf{S}_j\right]\right\}. \quad (18)$$

Here, $\mathbf{S}_i$ is the spin of quark i and α_s a normalization factor, treated as free parameter [17].

The hyperfine interaction generates the configuration mixing among the ground-state $N^2S_S([56, O^+])$ and other configurations, e.g., $N^2S'_S([56', O^+])$, N^2S_M ($[70, O^+]$), and N^4D_M ($[70, 2^+]$). Here, the notation is $X^{2S+1}L_\pi$, where $X = N, \Delta, \Sigma, \ldots, S$ the total quark spin, $L = S, P, D\ldots$ the total orbital angular momentum, and $\pi = S, M$, or A the permutational symmetry (symmetric, mixed symmetry, or antisymmetric, respectively) of the spatial wave function.

The first two terms in Eq. (17) can be rewritten as two harmonic oscillators within the Jocabi coordinate. Its solution is the well-known SU(6)⊗O(3) wave function. The breakdown of the symmetry arises from the additional terms. Given that the configuration mixing is mainly produced by the spin- and flavor-dependent parts of Hamiltonian [32], here we use a simple method to deal with the confinement terms in Refs. [11,18], where three constants E_0, Ω, and Δ are introduced.

To illustrate the modifications of the scattering amplitudes due to the SU(6)⊗O(3) symmetry breakdown, we give in the following the explicit derivations in the case of the $S_{11}(1535)$ resonance. In lines with Ref. [40], we express the amplitudes $\mathcal{A}_{S_{11}}$ in terms of the product of the photoexcitation and meson-decay transition amplitudes,

$$\mathcal{A}_{S_{11}} \propto \langle N|H_m|S_{11}\rangle\langle S_{11}|H_e|N\rangle, \quad (19)$$

where H_m and H_e are the meson and photon transition operators, respectively. The wave function can be written within the SU(6)⊗O(3) symmetry for $n \leqslant 2$ shells as $X^{2S+1}L_\pi J^P$ and configuration mixing, with J^P the state's total angular momentum and parity,

$$|S_{11}(1535)\rangle = -\sin\theta_S\left|N^4P_M\tfrac{1}{2}^-\right\rangle + \cos\theta_S\left|N^2P_M\tfrac{1}{2}^-\right\rangle, \quad (20)$$

$$|\text{Nucleon}\rangle = c_1\left|N^2S_S\tfrac{1}{2}^+\right\rangle + c_2\left|N^2S'_S\tfrac{1}{2}^+\right\rangle + c_3\left|N^4D_M\tfrac{1}{2}^+\right\rangle + c_4\left|N^2S_M\tfrac{1}{2}^+\right\rangle + c_5\left|N^2P_A\tfrac{1}{2}^+\right\rangle, \quad (21)$$

where θ_S and c_i can be determined by the OGE model. If we set $c_1 = 1$ and $c_{2,3,4,5} = 0$ (so $\theta_S = 0$), then the SU(6)⊗O(3) symmetry is restored. The improvement compared to Ref. [40] is that here we take into account the mixing not only in the intermediate S_{11} resonance but also in the initial- and final-state nucleon. Moreover, for other resonances, we also include directly the configuration mixing of wave functions via OGE model so we do not need to introduce the free parameters C_{N^*} [Eq. (16)].

The electromagnetic transition amplitudes then take the following form:

$$\begin{aligned}\langle S_{11}|H_e|N\rangle &= c_1\left\langle S_{11}\left|H_e\right|N^2S_S\tfrac{1}{2}^+\right\rangle + c_2\left\langle S_{11}\left|H_e\right|N^2S'_S\tfrac{1}{2}^+\right\rangle \\ &\quad + c_3\left\langle S_{11}\left|H_e\right|N^4D_M\tfrac{1}{2}^+\right\rangle + c_4\left\langle S_{11}\left|H_e\right|N^2S_M\tfrac{1}{2}^+\right\rangle \\ &\quad + c_5\left\langle S_{11}\left|H_e\right|N^2P_A\tfrac{1}{2}^+\right\rangle \\ &= c_1\cos\theta\left\langle N^2P_M\tfrac{1}{2}^-\left|H_e\right|N^2S_S\tfrac{1}{2}^+\right\rangle + \cdots. \end{aligned} \quad (22)$$

Here, the term $\langle N^4P_M\frac{1}{2}^-|H_e|N^2S_S\frac{1}{2}^+\rangle$ vanishes because of the Moorhouse rule [55]. In Ref. [40], the mixing angles are introduced also to give a nonzero value for contributions from the $D_{13}(1700)$ resonance, but the nucleon wave function includes only the $n = 0$ part, that is, $c_1 = 1, c_{2,3,4,5} = 0$. Moreover, the contribution of the $D_{15}(1675)$ ($|N^4D_M\frac{5}{2}^+\rangle$ state) is zero, if we consider only the wave function up to $n = 2$. Then, in Ref. [40], for this latter resonance a term identical to the contribution to the η photoproduction on neutron target was added by hands. In this work, the nucleon wave function with $n = 2$ produces *naturally* a nonzero contribution with the same form as for neutron target under the SU(6)⊗O(3) symmetry.

Analogously, for meson decay amplitudes we get,

$$\langle N|H_m|S_{11}\rangle = c_1(\cos\theta_S - \mathcal{R}\sin\theta_S) \times\left\langle N^2S_S\tfrac{1}{2}^+\left|H_m\right|N^2P_M\tfrac{1}{2}^-\right\rangle + \cdots \quad (23)$$

and the ratio

$$\mathcal{R} = \frac{\left\langle N|H_m|N(^4P_M)_{\frac{1}{2}^-}\right\rangle}{\left\langle N|H_m|N(^2P_M)_{\frac{1}{2}^-}\right\rangle}, \quad (24)$$

is a constant determined by the SU(6)⊗O(3) symmetry.

Then, Eq. (19) reads,

$$\mathcal{A}_{S_{11}} = C_{S_{11}}\left\langle N^2S_S\tfrac{1}{2}^+|H_m|N^2P_M\tfrac{1}{2}^-\right\rangle \times\left\langle N^2P_M\tfrac{1}{2}^-|H_e|N^2S_S\tfrac{1}{2}^+\right\rangle + \cdots, \quad (25)$$

where

$$C_{S_{11}} = c_1^2\left(\cos^2\theta_S - \mathcal{R}\sin\theta_S\cos\theta_S\right) + \cdots. \quad (26)$$

So, if we remove all $n = 2$ parts from the wave function of the nucleon, as in Ref. [39], then the factor $C_{S_{11}}$ is a constant. However, after other contributions are included, it becomes dependent on the momenta k and q. In this work we keep this dependence.

III. RESULTS AND DISCUSSION

With the formalism presented in Sec. II, we investigate the process $\gamma p \to \eta p$. A chiral constituent quark model was proven [40] to be an appropriate approach to that end. That

work embodied one free parameter per nucleon resonance to take into account the breaking of the SU(6)⊗O(3) symmetry. In the present work, this latter phenomenon is treated via configuration mixing, reducing the number of adjustable parameters. As in Ref. [40], we introduce resonances in $n \leqslant 2$ shells to study the η photoproduction in the center-of-mass energy $W \leqslant 2$ GeV.

A. Fitting procedure

Using the CERN MINUIT code, we have fitted simultaneously the following data sets:

(i) **Differential cross section:** Database includes 1220 data points for $1.49 \lesssim W \leqslant 1.99$ GeV from the following labs: MAMI [1], CLAS [2], ELSA [3], LNS [4], and GRAAL [5]. Only statistical uncertainties are used.

(ii) **Polarized beam asymmetry:** Polarized beam asymmetries (184 data points) for $1.49 \lesssim W \leqslant 1.92$ GeV from GRAAL [5] and ELSA [6]. Only statistical uncertainties are used.

(iii) **Spectrum of known resonances:** For spectrum of known resonances, we use as input their PDG values [26] for masses and widths, with the uncertainties reported there plus an additional theoretical uncertainty of 15 MeV, as in Ref. [21], to avoid overemphasis of the resonances with small errors. The database contains all 12 known nucleon resonances as in PDG, with $M \leqslant$ 2 GeV, namely

$\boldsymbol{n} = 1$: $S_{11}(1535)$, $S_{11}(1650)$, $D_{13}(1520)$, $D_{13}(1700)$ and $D_{15}(1675)$

$\boldsymbol{n} = 2$: $P_{11}(1440)$, $P_{11}(1710)$, $P_{13}(1720)$, $P_{13}(1900)$, $F_{15}(1680)$, $F_{15}(2000)$ and $F_{17}(1990)$

In addition to the above isospin-1/2 resonances, we fitted also the mass of $\Delta(1232)$ resonance. However, spin-3/2 resonances do not intervene in η photoproduction.

(iv) **Additional resonance:** Resonances with masses above $M \approx 2$ GeV, treated as degenerate, are simulated by a single resonance, for which the mass, the width, and the symmetry-breaking coefficient are left as adjustable parameters.

The adjustable parameters, listed in Table I, are as follows: η nucleon coupling ($g_{\eta NN}$), mass of the nonstrange quarks (m_q), harmonic oscillator strength (α), QCD coupling constant (α_s), confinement constants (E_0, Ω, and Δ), three parameters M, Γ, and C_N^* related to the degenerate treatment of resonances with masses above ≈2 GeV, and the strength of the $P_{13}(1720)$ resonance. We will come back to this latter parameter.

The spectrum of the known resonances put constraints on six of the adjustable parameters. Five of them (m_q, α, α_s, Ω, and Δ) are determined through an interplay between the mass spectrum of the resonances and the photoproduction data via the configuration mixings parameters c_i [Eq. (22)] reported in Appendix. The sixth one, E_0, is determined by the mass of nucleon. The coupling constant $g_{\eta NN}$ is determined by photoproduction data. The parameter $C_{P_{13}(1720)}$ is the strength of the $P_{13}(1720)$ resonance that we had to treat as adjustable to avoid its too-large contribution resulting from direct calculation. This latter parameter, as well as those defining the higher mass resonance (HM N^*) are determined by the photoproduction data. Note that, in fitting the photoproduction data, we use the PDG [26] values for masses and widths of resonances.

TABLE I. Adjustable parameters and their extracted values, with m_q, α, E_0, Ω, Δ, M, and Γ in MeV.

	Parameter	Model A	Model B
	$g_{\eta NN}$	0.391	0.449
	m_q	277	304
	α	288	285
	α_s	1.581	1.977
	E_0	1135	1138
	Ω	450	442
	Δ	460	460
	$C_{P_{13}(1720)}$	0.382	0.399
HM N^*:			
	M	1979	2129
	Γ	124	80
	C_{N^*}	−0.85	−0.70
New S_{11}:			
	M		1717
	Γ		217
	C_{N^*}		0.59
New D_{13}:			
	M		1943
	Γ		139
	C_{N^*}		−0.19
New D_{15}:			
	M		2090
	Γ		328
	C_{N^*}		2.89
χ^2_{DOF}		12.37	2.31

The complete set of adjustable parameters mentioned above leads to our model A; see the third column in Table I, for which the reduced χ^2 turns out to be large (12.37).

In recent years, several authors [9,40,42–51] have put forward need for new resonances in interpreting various observables, with extracted masses roughly between 1.73 and 2.1 GeV. We have hence, investigated possible contributions from three of them: S_{11}, D_{13}, and D_{15}. For each of those new resonances we introduce then three additional adjustable parameters per resonance: mass (M), width (Γ), and symmetry-breaking coefficient (C_{N^*}). Fitting the same database, we obtained a second model, called model B, for which the adjustable parameters are reported in the last column of Table I. The reduced χ^2 is very significantly improved going down from 12.37 to 2.31. In the rest of this section, we concentrate on model B.

Extracted values within OGE model come out close to those used by Isgur-Karl [18] and Capstick-Roberts [11]: $E_0 =$ 1150 MeV, $\Omega \approx 440$ MeV, $\Delta \approx 440$ MeV. For three other parameters, Isgur and Capstick introduce $\delta = (4\alpha_s\alpha)/(3\sqrt{2\pi}m_u^2)$, for which they get ≈300 MeV. Model B gives $\delta \approx 262$ MeV.

TABLE II. Extracted masses for known resonances. For each resonance, results of the present work (M^{OGE}) are given in the first line, predictions from Isgur and Karl for negative-parity [17] and positive-parity [18] excited baryons in the second line, and PDG values [26] in the third line.

	$S_{11}(1535)$	$S_{11}(1650)$	$P_{11}(1440)$	$P_{11}(1710)$	$P_{13}(1720)$	$P_{13}(1900)$
M^{OGE}	1473	1620	1428	1723	1718	1854
Refs. [17,18]	1490	1655	1405	1705	1710	1870
M^{PDG}	1535 ± 10	1655^{+15}_{-10}	1440^{+30}_{-20}	1710 ± 30	1720^{+30}_{-20}	1900
	$D_{13}(1520)$	$D_{13}(1700)$	$D_{15}(1675)$	$F_{15}(1680)$	$F_{15}(2000)$	$F_{17}(1990)$
M^{OGE}	1511	1699	1632	1723	2008	1945
Refs. [17,18]	1535	1745	1670	1715	2025	1955
M^{PDG}	1520 ± 5	1700 ± 50	1675 ± 5	1685 ± 5	2000	1990

For the three new resonances, we follow the method in Ref. [39], as discussed in Sec. II B, via Eq. (16). The extracted Wigner mass and width, as well as the strength for those resonances are given in Table I.

For the new S_{11}, the Wigner mass and width are consistent with the values in Refs. [40,43,44,51], but the mass is lower, by about 100 to 200 MeV, than findings by other authors [22,42,46–48]. The most natural explanation would be that it is the first S_{11} state in the $n = 3$ shell; however, its low mass could indicate a multiquark component, such as a quasibound kaon-hyperon [43] or a pentaquark state [56]. For the $D_{13}(1850)$, the variation of χ^2 is small. Interestingly, we find large effect from a D_{15} state around 2090 GeV with a Wigner width of 330 MeV. It is very similar to the $N(2070)D_{15}$ reported in Refs. [3,9]. It can be explained as the first D_{15} state in $n = 3$ shell [3].

The results of baryon spectrum extracted from the present work are reported in Tables II and III. Table II is devoted to the known resonances. Our results are in good agreement with those obtained by Isgur and Karl [17,18], and except for the $S_{11}(1535)$ and $D_{13}(1520)$, fall in the ranges estimated by PDG [26]. As mentioned in Introduction, issues related to extracted masses via models and those compiled by the PDG are under investigation [25]. The additional "missing" resonances generated by the OGE model are shown in Table III. The extracted masses are compatible with those reported by Isgur and Karl [17,18].

In Table IV, we examine the sensitivity of our model to its ingredients by switching off one resonance at a time and noting the χ^2, without further minimizations. As expected, the most important role is played by the $S_{11}(1535)$, and the effects of $S_{11}(1650)$ and $D_{13}(1520)$ turn out to be very significant. Within the known resonances, the other two ones contributing largely enough are $F_{15}(1680)$ and $P_{13}(1720)$. In addition to those five known resonances, a new S_{11} appears to be strongly needed by the data, whereas the smaller effect of a new D_{15} is found to be non-negligible. Finally, higher mass resonance ($M \gtrsim 2$ GeV) and a new D_{13} do not bring in significant effects.

TABLE III. Predicted masses for "missing" negative-parity excited baryon by the present work (M^{OGE}) and by Isgur and Karl [18].

	P_{11}	P_{11}	P_{13}	P_{13}	P_{13}	F_{15}
M^{OGE}	1899	2051	1942	1965	2047	1943
Ref. [18]	1890	2055	1955	1980	2060	1955

Our model B is built on resonances given in Table IV. In Table V we investigate possible contributions from the missing resonances (Table III). Here, we add them one by one to model B without further minimizations. As reported in Table V, none of them play a noticable role in the reaction mechanism. Please note that for those resonances we use the masses that we have determined. We have checked the changes of the χ^2 by varying those masses by ± 100 MeV. Moreover, given that there is no unique information available on their widths, we let them vary between 100 MeV and 1 GeV. The effects of those procedures on the reported χ^2s (Table V) come out to be less than 10%.

After having discussed above the s-channel contribution, we end this section with a few comments. In our models, nonresonant components include a nucleon pole term and u-channel contributions, treated as degenerate to the harmonic oscillator shell n. t-channel contributions due to the ρ and ω exchanges [57], found [58] to be negligible, are not included in the present work. Our finding about the effect of higher mass resonances being very small supports the neglect of the t channel, due to the duality hypothesis (see, e.g., Refs. [40,59]).

Finally, the target asymmetry (T) data [60] are not included in our database. Actually, those 50 data points bear too large uncertainties to put significant constraints on the parameters [58].

B. Differential cross section and Beam asymmetry

In Figs. 1, 2, and 3, we report our results for angular distributions of differential cross sections, excitation functions, and polarized-beam asymmetries (Σ), respectively. Results for models A and B are shown in all three figures. The first striking point is that model A compares satisfactorily with data up to $W \lesssim 1.65$ GeV but shows very serious shortcomings above, especially in the range W ≈ 1.7 to 1.8 GeV. Model B reproduces the differential cross-section and polarization

TABLE IV. The χ^2s shown are the values after turning off the corresponding (known) resonance contribution within the model B, for which $\chi^2 = 2.31$.

Removed N^*	$S_{11}(1535)$	$S_{11}(1650)$	$P_{11}(1440)$	$P_{11}(1710)$	$P_{13}(1720)$	$P_{13}(1900)$
χ^2	162	11.9	2.29	2.39	4.15	2.35
Removed N^*	$D_{13}(1520)$	$D_{13}(1700)$	$D_{15}(1675)$	$F_{15}(1680)$	$F_{15}(2000)$	$F_{17}(1990)$
χ^2	9.83	2.29	2.24	4.82	2.33	2.31
Removed N^*	HM N^*	New S_{11}	New D_{13}	New D_{15}		
χ^2	2.50	12.69	2.63	3.88		

data well enough, though some discrepancies appear at the highest energies and most forward angles ($W \gtrsim 1.85$ and $\theta \lesssim 50^\circ$).

In Fig. 1, we concentrate on the role played by the three most relevant known resonances discussed in Sec. III A (see Table IV), namely by removing one resonance at a time within model B. The $S_{11}(1535)$ is by far the most dominant resonance at lower energies and has sizable effects up to $W \approx 1.8$ GeV, whereas the $S_{11}(1650)$ shows significant contributions only at intermediate energies. The $D_{13}(1520)$ has less significant contribution, but its role is crucial in reproducing the correct shape of the differential cross section, especially at intermediate energies.

The importance of the other two known resonances, leading to a significant increase of χ^2 when switched off (see Table IV) are illustrated in the left panel of Fig. 2. Although the $P_{13}(1720)$ affects extreme angles around $W \approx 1.8$ GeV, the $F_{15}(1680)$ is visible only at a forward angle.

The right panel of Fig. 2 is devoted to the roles played by the three new resonances. As mentioned above, the main shortcoming of model A appears around $W \approx 1.7$–1.8 GeV. This undesirable feature is cured in model B, due mainly to the new S_{11}, the mass of which turns out to be $M = 1.717$ GeV. Figure 2 illustrates the increase of χ^2 (Table IV) when that resonance is switched off in model B. Smaller contributions from the new D_{15} appear in the forward hemisphere, whereas the new D_{13} has no significant manifestation.

Polarized-beam asymmetry results are reported in Fig. 3. As shown in the left panel of that figure, although model B gives a better account of the data than model A, the contrast is less important compared to the differential cross-section observable. The $S_{11}(1535)$ continues playing a primordial role, whereas the effect of $S_{11}(1650)$ tends to be marginal. This is also the case (middle panel) for the known $P_{13}(1720)$ and missing $P_{13}(1942)$. The established importance of the $D_{13}(1520)$ and $F_{15}(1680)$ (in left and middle panels, respectively) within this observable appear clearly.

In the right panel of Fig. 3, we examine the case of three new resonances. The new S_{11} gives sizable contributions in the energy range corresponding roughly to its mass. In contrast to the differential cross section, the new D_{13} appears to be significant in the backward hemisphere. Finally, switching off the new D_{15} improves the agreement with the data at most backward angles shown, whereas for the cross section we get an opposite behavior. This isolated contradiction reflects the relative weight of data for the two observables (roughly six times more differential cross-section data than polarization asymmetry, with comparable accuracies).

This section, devoted to the observables of the the process $\gamma p \to \eta p$, in the energy range $W \lesssim 2$ GeV, leads to the conclusion that within our approach, the reaction mechanism is dominated by five known and two new nucleon resonances.

C. Helicity amplitudes and partial decay width

As discussed in Sec. IV [Eqs. (20), (21), and (25)], our approach allows calculating the helicity amplitudes and the partial decay width $N^* \to \eta N$ within a given model without further adjustable parameters.

In Table VI we report on our results within model B, for all $n = 1$ and 2 shell resonances generated by the quark model and complemented with the OGE model. In that table, the second and fourth columns show our results for the helicity amplitudes. Those amplitudes are in line with results from other similar approaches (see Tables I and II in Ref. [11]).

Comparing our results for the dominant known resonances of model B with values reported in PDG [26] (third and fifth columns in Table VI) leads to following remarks: (i) $A_{1/2}$ amplitudes for $S_{11}(1535)$ and $S_{11}(1650)$, as well as $A_{1/2}$ and $A_{3/2}$ for $D_{13}(1520)$ and $A_{3/2}$ for $F_{15}(1680)$ are in good agreement with the PDG values. For this latter resonances

TABLE V. The χ^2s shown are the values after adding the corresponding (missing) resonance contribution within model B, for which $\chi^2 = 2.31$.

Added N^*	$P_{11}(1899)$	$P_{11}(2051)$	$P_{13}(1942)$	$P_{13}(1965)$	$P_{13}(2047)$	$F_{15}(1943)$
χ^2	2.31	2.31	2.26	2.31	2.32	2.28

TABLE VI. Helicity amplitudes and decay widths for resonances, with $\Gamma_{\eta N}^{\rm PDG} = \Gamma_{\rm tot} \cdot {\rm Br}_{\eta N}$ in PDG [26].

Resonances	$A_{1/2}$	$A_{1/2}^{\rm PDG}$	$A_{3/2}$	$A_{3/2}^{\rm PDG}$	$\sigma\sqrt{\Gamma_{\eta N}}$	$(\sigma)\sqrt{\Gamma_{\eta N}^{\rm PDG}}$
$S_{11}(1535)$	72	90 ± 30			7.05	$(+)8.87^{+1.37}_{-1.37}$
$S_{11}(1650)$	60	53 ± 16			-2.20	$1.95^{+0.94}_{-1.57}$
$P_{11}(1440)$	37	-65 ± 4				
$P_{11}(1710)$	27	9 ± 22			1.30	$2.49^{+1.75}_{-0.88}$
P_{11}	3				-1.64	
P_{11}	-2				-0.76	
$P_{13}(1720)$	194	18 ± 30	-72	-19 ± 20	2.07	$2.83^{+1.04}_{-0.71}$
$P_{13}(1900)$	33		1		-0.87	$8.35^{+2.11}_{-2.20}$
P_{13}	32		-2		1.80	
P_{13}	14		2		0.05	
P_{13}	-4		4		-0.73	
$D_{13}(1520)$	-20	-24 ± 9	144	166 ± 5	0.30	$0.51^{+0.07}_{-0.06}$
$D_{13}(1700)$	-6	-18 ± 13	2	-2 ± 24	-0.57	$0.00^{+1.22}_{-0.00}$
$D_{15}(1675)$	-6	19 ± 8	-9	15 ± 9	-1.74	$0.00^{+1.28}_{-0.00}$
$F_{15}(1680)$	14	-15 ± 6	142	133 ± 12	0.44	$0.00^{+1.18}_{-0.00}$
F_{15}	-12		5		0.78	
$F_{15}(2000)$	-1		13		-0.38	
$F_{17}(1990)$	6	1	8	4	-1.25	$0.00^{+2.17}_{-0.00}$

the $A_{1/2}$ has the right magnitude but the opposite sign with respect to the PDG value. However, for that resonance $A_{3/2}$ being much larger than $A_{1/2}$, the effect of this latter amplitude is not significant enough in computing the observables. The amplitudes for $P_{13}(1720)$ deviate significantly from their PDG values, as it is the case in other relevant approaches (see Table II in Ref. [11]). Those large values produced by our model forced us to leave the symmetry breaking coefficient for $P_{13}(1720)$ as a free parameter (Table I) to suppress its otherwise too-large contribution. As much as other known resonances are concerned we get results compatible with the PDG values for $D_{13}(1700)$ and $F_{17}(1990)$ and to a lesser extent for $D_{15}(1675)$. For $P_{11}(1440)$ our value deviates significantly from the PDG one. Once again, our result confirms the general trend observed in other works (see Table II in Ref. [11]), which very likely reflects the still unknown structure of that

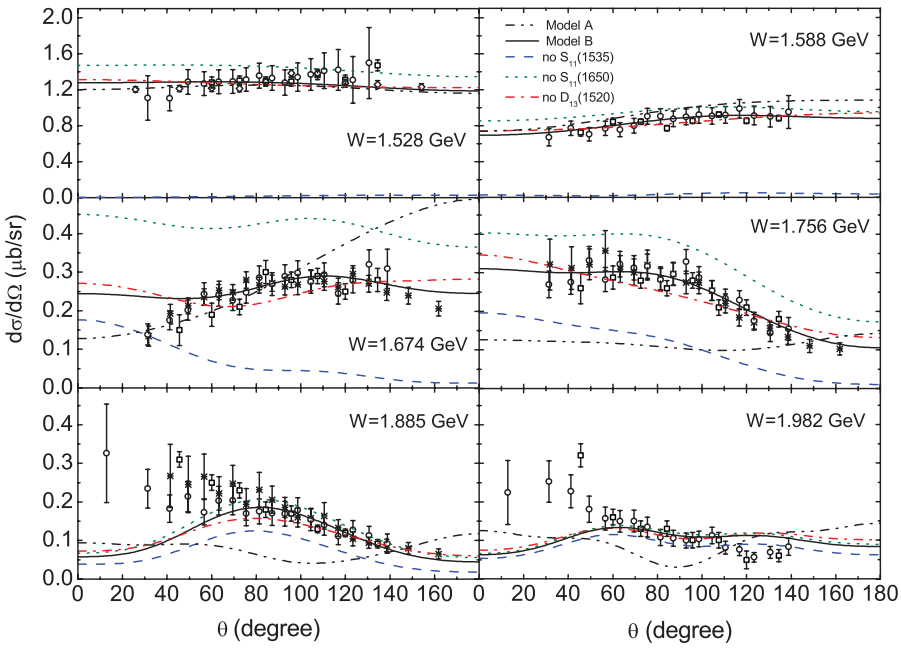

FIG. 1. (Color online) Differential cross section for the process $\gamma p \to \eta p$. The curves are for models A (dash-dot-dotted) and B (full). The other curves are obtained within model B by switching off one resonances at a time: $S_{11}(1535)$ (dashed), $S_{11}(1650)$ (dotted), and $D_{13}(1520)$ (dash-dotted). The data are from CLAS (squares) [2], ELSA (circles) [3], Mainz (diamonds) [1], and GRAAL (stars) [5].

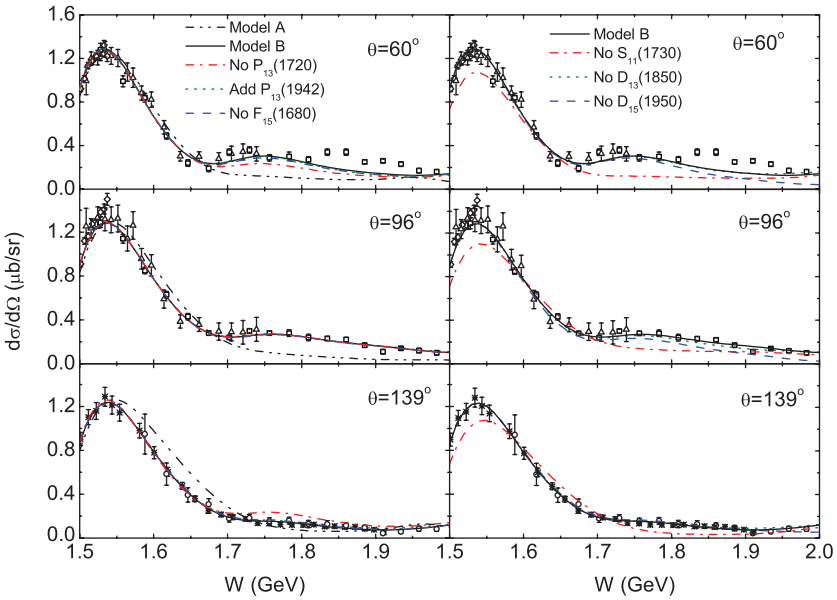

FIG. 2. (Color online) Differential cross section for the process $\gamma p \to \eta p$ as a function of W at three angles. The dash-dot-dotted and full curves correspond to models A and B. All other curves are obtained within model B by turning off one known resonance or adding a missing one. (Left panel) Switching off $P_{13}(1720)$ (dash-dotted), $F_{15}(1680)$ (dashed); adding $P_{13}(1942)$ (dotted). (Right panel) Switching off $S_{11}(1730)$ (dash-dotted), $D_{13}(1850)$ (dotted), $D_{15}(1950)$ (dashed). The data are from CLAS (squares) [2], Mainz (diamonds) [1], LNS (uptriangles) [4].

resonance. Finally, we put forward predictions also for the missing resonances, for which we find rather small amplitudes, explaining the negligible roles played by them in our model.

The sixth and seventh columns in Table VI show our results and PDG values, respectively, for the partial decay widths of resonances decay in the ηN channel, where σ is the sign for $\pi N \to \eta N$ as in Ref. [19]. Notice that the sign (σ) in the PDG is known only for $S_{11}(1535)$. Except for the two star resonance $P_{13}(1900)$, the theoretical results are close to the PDG values.

It is worthwhile noting that all dominated resonances in our model B have large helicity amplitudes, whereas some of them turn out to have rather small decay widths to the ηN channel. This result indicates that in looking for appropriate reactions to search for missing resonances it is not enough to have rather sizable decay width, but one needs to put forward predictions for the observables.

IV. SUMMARY AND CONCLUSIONS

A formalism bringing together a chiral constituent quark approach and one-gluon-exchange model was presented and used to derive photoexcitation helicity amplitudes and partial decay width of the nucleon resonances.

Our approach gives a reasonable account of the measured observables for the process $\gamma p \to \eta p$ from threshold to $W \approx 2$ GeV. Among the 12 nucleon resonances in that energy range, compiled by PDG, 5 of them are found to play crucial roles in the reaction mechanism, namely $S_{11}(1535)$, $S_{11}(1650)$, $P_{13}(1720)$, $D_{13}(1520)$, and $F_{15}(1680)$. However, those known resonances led to our model A, which

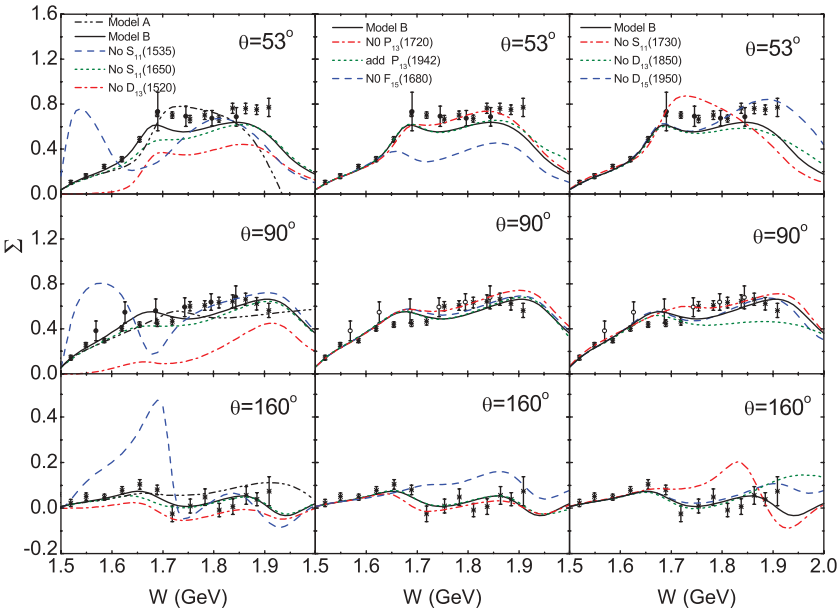

FIG. 3. (Color online) Polarized beam asymmetry for the process $\vec{\gamma} p \to \eta p$ as a function of W. The curves in the left panel are as in Fig. 1, and those in middle and right panels as in Fig. 2. The data are from ELSA (full circles) [6] and GRAAL (stars) [5].

does not allow an acceptable description of the data. Five extra resonances generated by the formalism, and known as missing resonances, turn out to show no significant contributions to the process under investigation. However, two new resonances reported in the literature, S_{11} and D_{15}, are found relevant to that process; the most important effect comes from the S_{11} resonance. We extracted the mass and width of those resonances: S_{11} (1.730 GeV, 217 MeV), and D_{15} (2.090 GeV, 328 MeV). Our model B, embodying those latter resonances, describes successfully the data.

The helicity amplitudes and decay widths are calculated with the same parameters. Our results are compatible with other findings and come out close to the PDG values in most cases.

To go further, we are pursing our investigations in two directions:

(i) In the present work the s-channel resonances with masses above 2 GeV were treated as degenerate, given that the transition amplitudes, translated into the standard CGLN amplitudes, were restricted to harmonic oscillator shells, $n \leqslant 2$. Recently, we have extended our formalism and derived explicitly the amplitudes also for $n = 3$ to 6 shells. Model search, including *all* known one- to four-star resonances in PDG, for $W \approx 2.6$ GeV is in progress [58].

(ii) Our constituent quark approach applied to the $\gamma p \to K^+\Lambda$ channel [61] showed that the intermediate meson-baryon states, treated within a coupled-channels formalism [62], have significant effects on the photoproduction observables [51]. A more sophisticated coupling-channels treatment [63] was developed and was applied to the η photoproduction reaction. Results of that work will be reported elsewhere.

ACKNOWLEDGMENT

We are deeply grateful to Qiang Zhao for enlightening discussions.

APPENDIX: MIXING COEFFICIENTS OF THE WAVE FUNCTIONS

In Table VII, we present the mixing coefficients of the wave functions. Isgur and Karl [16,18] have given their explicit values for positive-parity and negative-parity resonances, respectively. But in Ref. [16] the mixing between $n = 0$ and $n = 2$ shells is not considered. Such mixings for the ground state are given in Ref. [19] without the contribution of ^2P_A. The parameters in that reference are determined only by the mass spectrum. Here we give our results by fitting both the mass spectrum and the η photoproduction observables. In calculation we follow the conventions in Ref. [19].

The mixing coefficients reported here lead to mixing angles $\Theta_S = -31.7^\circ$ and $\Theta_D = 6.4^\circ$, in agreement with results from other authors [15,34,64,65].

TABLE VII. Mixing coefficients of the wave functions.

State	Wave function($^{2S+1}L_\pi$)				
S_{11}	^2P_M	^4P_M			
$N(1535)$	−0.851	0.526			
$N(1650)$	0.526	0.851			
P_{11}	^2S_S	^4D_M	^2P_A	$^2S'_S$	^2S_M
$N(938)$	0.941	−0.043	−0.002	−0.260	−0.211
$N(1440)$	0.268	0.000	0.000	0.964	0.006
$N(1710)$	0.175	−0.343	−0.071	−0.054	0.919
	−0.103	−0.839	−0.424	0.031	−0.324
$N(2100)$	−0.032	−0.421	0.903	0.010	−0.080
P_{13}	^2D_S	^2D_M	^4D_M	^2P_A	^4S_M
$N(1720)$	0.858	−0.483	0.023	−0.003	−0.176
$N(1900)$	0.314	0.234	−0.365	0.095	0.839
	−0.185	−0.482	0.606	−0.333	0.505
	0.359	0.686	0.496	−0.387	−0.065
	−0.059	−0.096	−0.502	−0.854	−0.073
D_{13}	^2P_M	^4P_M			
$N(1520)$	−0.994	−0.111			
$N(1700)$	−0.111	0.994			
D_{15}	^4P_M				
$N(1675)$	1.000				
F_{15}	^2D_S	^2D_M	^4D_M		
$N(1680)$	0.883	−0.469	0.001		
	−0.457	−0.860	−0.225		
$N(2000)$	−0.107	−0.198	0.974		
F_{17}	^4D_M				
$N(1990)$	1.000				

[1] B. Krusche *et al.*, Phys. Rev. Lett. **74**, 3736 (1995).
[2] M. Dugger *et al.* (CLAS Collaboration), Phys. Rev. Lett. **89**, 222002 (2002).
[3] V. Crede *et al.* (CB-ELSA Collaboration), Phys. Rev. Lett. **94**, 012004 (2005).
[4] T. Nakabayashi *et al.*, Phys. Rev. C **74**, 035202 (2006).
[5] O. Bartalini *et al.* (GRAAL Collaboration), Eur. Phys. J. A **33**, 169 (2007).
[6] D. Elsner *et al.* (CB-ELSA and TAPS Collaborations), Eur. Phys. J. A **33**, 147 (2007).
[7] W.-T. Chiang, S. N. Yang, L. Tiator, M. Vanderhaeghen, and D. Drechsel, Phys. Rev. C **68**, 045202 (2003).
[8] T. Feuster and U. Mosel, Phys. Rev. C **59**, 460 (1999).
[9] A. V. Anisovich, A. Sarantsev, O. Bartholomy, E. Klempt, V. A. Nikonov, and U. Thoma, Eur. Phys. J. A **25**, 427 (2005); A. V. Sarantsev, V. A. Nikonov, A. V. Anisovich, E. Klempt, and U. Thoma, Eur. Phys. J. A **25**, 441 (2005).
[10] R. A. Arndt, W. J. Briscoe, I. I. Strakovsky, and R. L. Workman, Int. J. Mod. Phys. A **22**, 349 (2007).
[11] S. Capstick and W. Roberts, Prog. Part. Nucl. Phys. **45**, 5241 (2000), and references therein.

[12] L. A. Copley, G. Karl, and E. Obryk, Nucl. Phys. **B13**, 303 (1969).
[13] R. P. Feynman, M. Kislinger, and F. Ravndal, Phys. Rev. D **3**, 2706 (1971).
[14] A. De Rújula, H. Georgi, and S. L. Glashow, Phys. Rev. D **12**, 147 (1975).
[15] N. Isgur and G. Karl, Phys. Lett. **B72**, 109 (1977); N. Isgur, G. Karl, and R. Koniuk, Phys. Rev. Lett. **41**, 1269 (1978).
[16] N. Isgur and G. Karl, Phys. Lett. **B74**, 353 (1978).
[17] N. Isgur and G. Karl, Phys. Rev. D **18**, 4187 (1978).
[18] N. Isgur and G. Karl, Phys. Rev. D **19**, 2653 (1979).
[19] R. Koniuk and N. Isgur, Phys. Rev. D **21**, 1868 (1980) [Erratum-*ibid.* **23**, 818 (1981)].
[20] S. Capstick and N. Isgur, Phys. Rev. D **34**, 2809 (1986).
[21] S. Capstick, Phys. Rev. D **46**, 2864 (1992).
[22] S. Capstick and W. Roberts, Phys. Rev. D **49**, 4570 (1994).
[23] S. Capstick and W. Roberts, Phys. Rev. D **58**, 074011 (1998).
[24] D. Morel and S. Capstick, arXiv:nucl-th/0204014; D. Morel, Ph.D. thesis, Florida State University, 2004, arXiv:nucl-th/0204028, and references therein.
[25] S. Capstick *et al*., Eur. Phys. J. A **35**, 253 (2008).
[26] W. M. Yao *et al*. (Particle Data Group), J. Phys. G **33**, 1 (2006).
[27] L. Y. Glozman and D. O. Riska, Phys. Rep. **268**, 263 (1996); L. Ya. Glozman, Nucl. Phys. **A629**, 121c (1997), and references therein.
[28] N. Isgur, Phys. Rev. D **62**, 054026 (2000).
[29] L. Ya. Glozman, arXiv: nucl-th/9909021.
[30] H. R. Pang, J. L. Ping, F. Wang, and J. Goldman, Phys. Rev. C **65**, 014003 (2001).
[31] F. Wang, J.-L. Ping, H.-R. Pang, and J. T. Goldman, Mod. Phys. Lett. A **18**, 356 (2003).
[32] Jun He and Yu-Bing Dong, Nucl. Phys. **A725**, 201 (2003).
[33] Jian Liu, Jun He, and Y. B. Dong, Phys. Rev. D **71**, 094004 (2005).
[34] J. Chizma and G. Karl, Phys. Rev. D **68**, 054007 (2003).
[35] J. Chizma, Ph.D. thesis, The University of Guelph, 2004 (unpublished).
[36] He Jun and Dong Yu-bing, Phys. Rev. D **68**, 017502 (2003).
[37] Z. Li, H. Ye, and M. Lu, Phys. Rev. C **56**, 1099 (1997).
[38] A. Manohar and H. Georgi, Nucl. Phys. **B234**, 189 (1984).
[39] Z. Li and B. Saghai, Nucl. Phys. **A644**, 345 (1998).
[40] B. Saghai and Z. Li, Eur. Phys. J. A **11**, 217 (2001); B. Saghai and Z. Li, *Proceedings of NSTAR 2002 Workshop on the Physics of Excited Nucleons*, Pittsburgh, PA, 2002; edited by S. A. Dytman and E. S. Swanson (World Scientific, Singapore, 2003).
[41] R. Bijker, F. Iachello, and A. Leviatan, Ann. Phys. **236**, 69 (1994); **284**, 89 (2000), and references therein.
[42] M. M. Giannini, E. Santopinto, and A. Vassallo, Eur. Phys. J. A **12**, 447 (2001); *Proceedings of NSTAR 2002 Workshop on the Physics of Excited Nucleons*, Pittsburgh, PA, 2002; edited by S. A. Dytman and E. S. Swanson (World Scientific, Singapore, 2003).
[43] Zhenping Li and Ron Workman, Phys. Rev. C **53**, R549 (1996).
[44] M. Batinić, I. Dadic, I. Šlaus, A. Švarc, B. M. K. Nefken, and T. S. H. Lee, arXive: nucl-th/9703023.
[45] J.-Z. Bai *et al*. (BES Collaboration), Phys. Lett. **B510**, 75 (2001); M. Ablikim *et al*. (BES Collaboration), Phys. Rev. Lett. **97**, 062001 (2006); B. S. Zou (BES Collaboration), *Proceeding of the Workshop on the Physics of Excited Nucleons*, Grenoble, France, 2004, edited by J.-P. Bocquet, V. Kuznetsov, and D. Rebreyend (World Scientific, Singapore, 2004); Sh. Fang (BES Collaboration), Int. J. Mod. Phys. A **21**, 839 (2006).
[46] G.-Y Chen, S. Kamalov, S. N. Yang, D. Drechsel, and L. Tiator, Nucl. Phys. **A723**, 447 (2003).
[47] W. T. Chiang, S. N. Yang, M. Vanderhaeghen, and D. Drechsel, Nucl. Phys. **A723**, 205 (2003).
[48] V. A. Tryasuchev, Eur. Phys. J. A **22**, 97 (2004).
[49] T. Mart, A. Sulaksono, and C. Bennhold, arXiv: nucl-th/0411035.
[50] N. G. Kelkar, M. Nowakowski, K. P. Khemchandani, and S. R. Jain, Nucl. Phys. **A730**, 121 (2004).
[51] B. Juliá-Díaz, B. Saghai, T.-S. H. Lee, and F. Tabakin, Phys. Rev. C **73**, 055204 (2006).
[52] G. F. Chew, M. L. Goldberger, F. E. Low, and Y. Nambu, Phys. Rev. **106**, 1345 (1957).
[53] R. L. Walker, Phys. Rev. **182**, 1729 (1969).
[54] V. Chaloupka *et al*. (Particle Data Group), Phys. Lett. **B50**, 1 (1974).
[55] R. G. Moorhouse, Phys. Rev. Lett. **16**, 772 (1966).
[56] B. S. Zou, Nucl. Phys. **A790**, 110 (2007).
[57] M. Benmerrouche, N. C. Mukhopadhyay, and J. F. Zhang, Phys. Rev. D **51**, 3237 (1995).
[58] J. He, B. Saghai, Z. Li, Q. Zhao, and J. Durand, Eur. Phys. J. A **35**, 321 (2008); comprehensive paper in preparation.
[59] P. Collins, *An Introduction to Regge Theory and High Energy Physics* (Cambridge University Press, New York, 1977); B. Saghai and F. Tabakin, Phys. Rev. C **53**, 66 (1996).
[60] A. Bock *et al*., Phys. Rev. Lett. **81**, 534 (1998).
[61] B. Juliá-Díaz, B. Saghai, F. Tabakin, W. T. Chiang, T.-S. H. Lee, and Z. Li, Nucl. Phys. **A755**, 463 (2005).
[62] W.-T. Chiang, B. Saghai, F. Tabakin, and T.-S. H. Lee, Phys. Rev. C **69**, 065208 (2004).
[63] J. Durand, B. Juliá-Díaz, T.-S. H. Lee, B. Saghai, and T. Sato, Phys. Rev. C **78**, 025204 (2008).
[64] S. Capstick and W. Roberts, Fizika B **13**, 271 (2004).
[65] I. K. Bensafa, F. Iddir, and L. Semalala, arXiv: hep-ph/0511195.